Effect of Energy Resolution in Compton Scattered Radiation Imaging

M. K. Nguyen †, J. L. Delarbre †, T. T. Truong ♭, C. Driol ♭, and H. Zaidi ‡

***Abstract*—Recently emission imaging exploiting Compton scattered radiation has been shown to be a feasible three-dimensional imaging modality, in particular for medical imaging. It exhibits several advantageous features among which the possibility of acquiring data using a stationary detector, instead of a moving one as in standard emission tomography imaging modalities. But measurements of scattered photons require high energy resolution detectors. Nowadays progress in detector technology allows to reach higher and higher energy resolution [1]–[3]. In this work, we consider the effect on image reconstruction of the finite energy resolution ΔE of a realistic collimated gamma camera. Approximate reconstruction methods are used to evaluate the image quality of the reconstructed object. It was observed that when ΔE is very small, the relative mean quadratic error is rather stable with respect to increasing values of n, the number of energy channels detected, but it becomes fluctuating as ΔE gets larger and larger. Conversely for given n, the relative mean quadratic error increases with ΔE. Results obtained using a simple phantom are also presented for various values of n and ΔE.**

I. Introduction

Emission imaging using Compton scattered radiation has been established since 2002 [4]. The derivation of the basic principles of image formation using only scattered photons lead to the introduction of the Compounded Conical Radon Transform (CCRT), which turned out to be invertible and paved the way to three-dimensional (3D) object reconstruction. This has been tested by numerical simulations [5] and has shown potential for possible applications in nuclear medicine emission and transmission imaging [6]. It should be emphasized that this imaging concept requires cameras equipped with very high energy resolution detectors.

In this work, we consider the effect of the finite energy resolution ΔE of a realistic gamma camera on image reconstruction quality. Given that scattered photons of energies in the interval $[E - \Delta E/2, E + \Delta E/2]$ contribute to the image formation process, which is now modeled by a modified CCRT (mCCRT), we use the mCCRT to generate n sets of data (n is the number of energy channels).

For approximate image reconstruction, the known inversion formula of the CCRT is adapted to two cases: a point source and a 3D phantom.

† Equipes de Traitement des Images et du Signal (ETIS), UMR CNRS 8051 / Université de Cergy-Pontoise / ENSEA, 6 avenue du Ponceau, F-95014 Cergy-Pontoise Cedex, France, mai.nguyen-verger@u-cergy.fr

♭ Laboratoire de Physique Théorique et Modélisation (LPTM), UMR CNRS 8089 / Université de Cergy-Pontoise, 2 avenue Adolphe Chauvin, F-95302 Cergy-Pontoise Cedex, France, truong@u-cergy.fr

‡ Geneva University Hospital, Division of Nuclear Medicine, CH-1211 Geneva 4, Switzerland, habib.zaidi@hcuge.ch

II. Image formation

To focus on the studied topic, attenuation will not be taken into account and isotropic primary emission is assumed (Fig. 1). The number of photons hitting a scattering site $\mathbf{M}$ in the solid angle $d\Omega_M$, after being emitted from volume element dV_S around point source $\mathbf{S}$, where the activity density $f(\mathbf{S})$, is:

$$\frac{f(\mathbf{S})}{4\pi}\, dV_S\, d\Omega_M.$$

Then the scattered photon flux emerging from site $\mathbf{M}$ in the direction of $\mathbf{D}$ per unit time and per unit solid angle is given by

$$\frac{f(\mathbf{S})dV_S}{4\pi}\frac{1}{SM^2} n_e(\mathbf{M})\, r_e^2\, P(\omega)\, dV_M.$$

where $P(\omega)$ is the Klein-Nishina scattering probability, r_e the

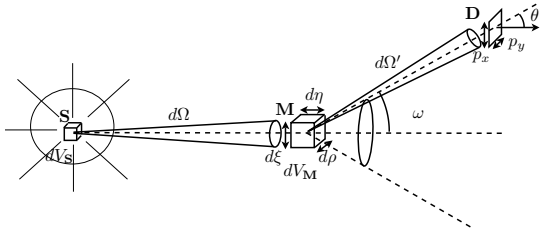

Fig. 1. Schematic diagram illustrating Compton scattering physical quantities and variables used in the mathematical formulation of the proposed approach.

classical electron radius and $n_e(\mathbf{M})$ the electron density.

The detected photon flux density at $\mathbf{D}$ is $g(\mathbf{D}, \omega)$ given by

$$g(\mathbf{D},\omega) = \int dx_M dy_M \frac{dz_M}{z_M^2}\delta(x_D - x_M)\delta(y_D - y_M) n_e(\mathbf{M}) \times \int \frac{f(\mathbf{S})dV_S}{4\pi}\frac{\delta(\text{cone})}{SM^2} r_e^2 P(\omega),$$

where $\delta(\text{cone})$ restricts the integration on $\mathbf{S}$ to a cone (Fig. 2).

$g(\mathbf{D}, \omega)$ is the Compounded Conical Radon Transform (CCRT) of $f(\mathbf{S})$. Now as the energy resolution is finite, one needs to perform a summation over ω in the interval $[E - \Delta E/2, E + \Delta E/2]$. The relationship between E and ω is given by the well known Compton formula. The measured quantity is actually

$$G(\mathbf{D}, \omega, \Delta E) = \int_{\Delta E} d\omega\, g(\mathbf{D}, \omega).$$

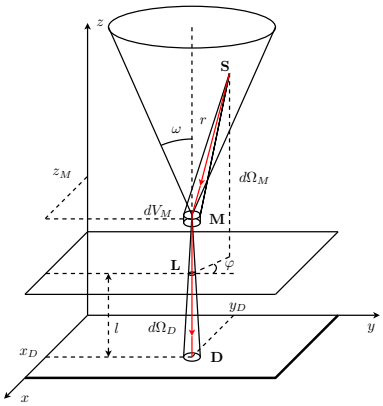

Fig. 2. Illustration of the Compounded Conical Radon Transform (CCRT).

This new integral transform is a modified Compounded Conical Radon Transform (mCCRT). To get an idea of the influence of the energy resolution, we adapt the inversion formula established for the CCRT to the data $G(\mathbf{D}, \omega, \Delta E)$ and study the deviation of the reconstructed object as compared to the original object as functions of ΔE.

III. Simulated imaging system

A. Detector module

We consider an imaging system equipped with a parallel hole collimated detector having the following characteristics:

- it is made of 64 $\times$ 64 square pixels of 3 mm size,
- the number of detected photons for each pixel are assigned to the pixel center, for each energy channel,
- the time unit is 10 seconds and the surface unit is the pixel area (9 mm^2),
- there are n energy channels between E_0, the primary emitted energy, and E_{n+1}, the backscattered energy. Thus for $i \in \{1...n\}$, the i^{th} channel energy is given by

$$E_i = \left(E_0 - \frac{E_0 - E_{n+1}}{2n}\right) - i.\Delta E.$$

B. Source and scattering medium

We consider an object consisting of an emitting cube made of 64 $\times$ 64 $\times$ 64 volume elements (voxels), each of them is a cube of side 3 mm. This object is immersed in a cubic scattering medium, the centers of the cubes are located on a same site and their sides parallel. The number of emitted photons per voxel and per unit time is assigned to its center. Moreover we assume that the detector plane is parallel to one cubical face of the scattering medium at a distance of 100 mm.

C. Numerical simulations

For each energy channel E_i and each detection site, we use the mCCRT to compute the received number of photons, as explained above. The number of photons, detected at a given energy inside a pixel is calculated as a weighted sum of the number of photons received par unit time and per unit area on points of the pixel.

The number of photons detected inside an energy interval in a pixel will also be calculated as a weighted sum of the number of photons received by a pixel for series of energy channels inside the energy interval chosen above.

In this study, we have performed simulations for the energy channels $E_n = \{64, 80, 96, 112, 128\}$ and for $\Delta E = \{0.1, 0.2, 0.4, 0.8, 1.2, 1.6, 2, 2.5, 3\}$ keV.

IV. Results

A. The two-dimensional case

In this section, we present the reconstruction results in the two dimensional case using numerical reconstruction methods (instead of using an approximate analytical inversion formula as in the 3D case) in order to evaluate the influence of energy resolution on image quality. The same assumptions remain valid throughout.

The square scattering medium has dimensions $X = 30$ cm $\times$ $Y = 15$ cm, which correspond to 64×32 voxels. The linear detector parallel to the square scattering medium along the X-direction has 96 linear pixels. We also consider $n = 32$ energy channels distributed from primary energy E_0 to backscattered energy E_{n+1}. The original objet is a square formed by 12 points in the middle of the scattering square medium. The most laborious task is the computation of the "weight" matrix in this numerical inversion procedure for implementation of the conjugate gradient reconstruction technique [7], [8]. The results are presented in Fig. 3.

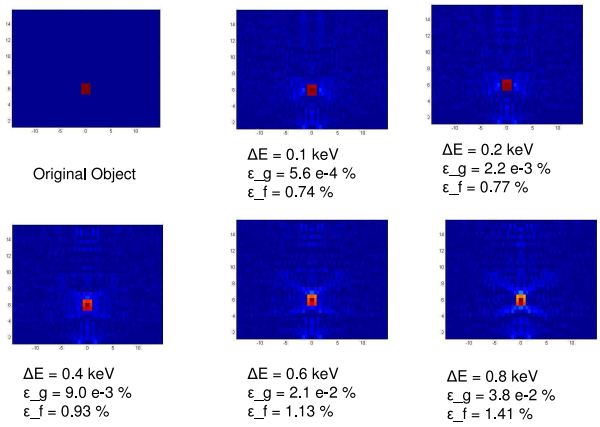

Fig. 3. Impact of energy resolution on reconstructed image quality.

To estimate the influence of energy resolution on reconstruction, we give the behavior of two metrics reflecting the error as a function of ΔE in Fig. 4.

- ϵ_f is the error between the original object and the reconstructed object,

- ϵ_g is the error between reconstructions with and without consideration of the finite energy resolution.

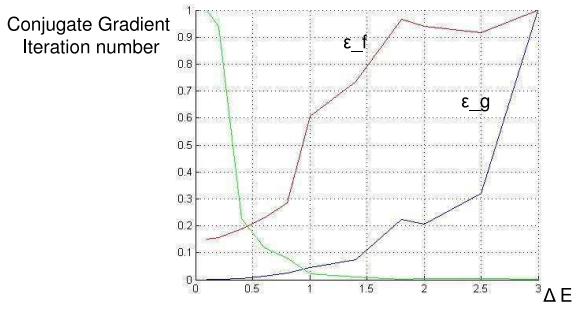

Fig. 4. Plots of ϵ_f, ϵ_g, and CG number of iterations as functions of ΔE

B. The three-dimensional case

1) Point source object: By assigning zero activity to all voxels except the center voxel of a cubic scattering medium, we simulate a point source for which we assign an activity corresponding to $131,868\,10^6$ photons emitted per unit time. To measure the reconstruction error as compared to the original object, we use two different quantities, the relative arithmetic mean error (ERAM) and the relative quadratic mean error (ERQM) given by the following equations:

$$ERAM_{max} = \frac{1}{M}\sum_{l=1}^{M}\frac{|O^*(l)-O(l)|}{\max_l O(l)}, \qquad (1)$$

and

$$ERQM_{max} = \sqrt{\frac{1}{M}\sum_{l=1}^{M}\left(\frac{O^*(l)-O(l)}{\max_l O(l)}\right)^2}, \qquad (2)$$

where M is the number of reconstructed voxels (here $64 \times 64 \times 64$), $O(l)$ the l[th] voxel of the original object and $O^*(l)$ the l[th] voxel of the reconstructed object.

The results for different values of ΔE and n for the point source simulation are summarized in Table 1.

2) 3D phantom object: To measure the reconstruction error, we introduce the related quantity:

$$ERAM = \frac{1}{M'}\sum_{l'=1}^{M'}\frac{|O^*(l')-O(l')|}{|O(l')|} \qquad (3)$$

ΔE	n=64	n=80	n=96	n=112	n=128
0.8	0.197	0.190	0.187	0.184	0.182
1.2	0.214	0.197	0.201	0.201	0.203
1.6	0.240	0.218	0.227	0.251	0.295
2	0.249	0.257	0.300	0.424	0.778
2.5	0.287	0.389	0.642	0.858	0.689
3	0.554	0.748	0.996	0.766	0.633

TABLE I
RECONSTRUCTION RELATIVE QUADRATIC MEAN ERROR($ERQM_max$)

$$ERQM = \sqrt{\frac{1}{M'}\sum_{l'=1}^{M'}\left(\frac{O^*(l')-O(l')}{O(l')}\right)^2} \qquad (4)$$

where M' is the number of voxels having non zero values, $O(l')$ is the l'[th] non zero voxel of the original object and $O^*(l')$ the l'[th] voxel of the reconstructed object.

Fig. 5 shows the original 3D phantom represented plane by plane. The two following figures (Figs. 6 and 7) illustrate reconstruction results for different values of the number of energy channels n and energy resolution ΔE. As can be seen on those examples, significant degradation of the image quality can occur when the energy resolution decreases.

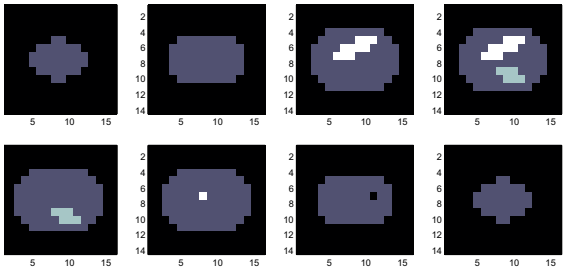

Fig. 5. Plane by plane representation of the original object.

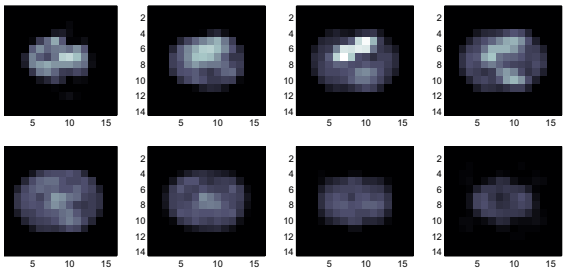

Fig. 6. Plane by plane representation of the reconstructed object for $n = 128$ and $\Delta E = 0.1$ keV.

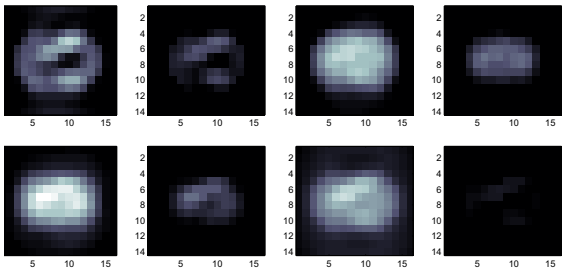

Fig. 7. Plane by plane representation of the reconstructed object for $n = 64$ and $\Delta E = 3$ keV.

V. Conclusion

As far as the point source study is concerned, we observe in both cases that for very small ΔE, the relative mean quadratic error is rather stable with respect to increasing values of n but it becomes fluctuating as ΔE gets larger and larger. Conversely for a given n, the relative mean quadratic error increases with ΔE. Therefore, it is clear that the image quality is strongly dependent on ΔE and the approach might find applications only on imaging systems with excellent energy resolution.

For the numerical phantom study, the effects of both n and of ΔE are similar. For $n \geq 96$ and $\Delta E \leq 0.4$, the reconstruction quality seems to be acceptable although blurred owing to the approximate reconstruction algorithm used. Again overall, it seems that ΔE is the most important disturbing factor affecting the resulting reconstructed image quality.

References

[1] W W Moses, *Current trends in scintillator detectors and materials* , Nucl. Inst. and Meth. Phys. Res. **A 487**, pp. 123-128, 2002.

[2] G Pellegrini, et. al. *Technology development of 3D detectors fro high-energy physics and imaging*, Nucl. Inst. and Meth. Phys. Res. **A 487**, pp. 19-26, 2002.

[3] C E Lehner, Z He nad F Zhang, 4π *Compton imaging using a 3D position sensitive CdZnTe detector via weighted listmode maximum likelihood*, IEEE Trans. Nucl. Sci. **51** (4), pp. 1618-1624, 2004.

[4] M. K. Nguyen and T.T. Truong, *On an Integral Transform and its Inverse in Nuclear Imaging*, Inverse Problems, Vol.**18** (1), pp. 265-277, 2002.

[5] M. K. Nguyen, T.T. Truong, H.D. Bui and J.L. Delarbre, *A novel inverse problem in gamma-ray emission imaging*, Inverse Problems in Science and Engineering, Vol.**12** (2), pp.225-246, 2004.

[6] M. K. Nguyen, T.T. Truong, J. L. Delarbre, C. Roux and H. Zaidi, *Novel approach to stationary transmission scanning using Compton scattered radiation*, Physics in Medicine and Biology, Vol.**52**, pp. 4615-4632, 2007.

[7] M. K. Nguyen, C. Driol, T. T. Truong and H. Zaidi, *Towards a new concept for high sensitivity Compton scatter emission imaging*, Journal of the European Optical Society: Rapid Publications, Vol.**3**, 08010 (2008), DOI: 10.2971/jeos.2008.08010.

[8] C. Driol, M. K. Nguyen and T. T. Truong, *Modeling and simulation results on high sensitivity scattered gamma-ray emission imaging*, Simulation Modelling Practice and Theory, Vol.**16** (8), pp. 1055-1066, 2008.